ACS EARTH AND SPACE CHEMISTRY

http://pubs.acs.org/journal/aesccq
Article

Laboratory Studies on the Influence of Hydrogen on Titan-like Photochemistry

Melissa S. Ugelow,* Scott T. Wieman, Madeline C. R. Schwarz, Victoria Da Poian, Jennifer C. Stern, and Melissa G. Trainer

Cite This: *ACS Earth Space Chem.* 2024, 8, 2362−2371
Read Online
ACCESS | Metrics & More | Article Recommendations

ABSTRACT: Laboratory investigations of photochemical reactions in simulated Titan-like atmospheric systems provide insight into the formation of gas and aerosol products and the influence of different environmental parameters on the types of organic molecules generated. Studying the gas-phase products as a function of reaction time provides further insight into the reaction pathways that lead to organic production. The stable isotopes in the reactants and products serve as tracers and help to disentangle these reaction pathways. We report a time study on the chemical composition and relative abundance of the evolved gas-phase products formed by far-ultraviolet reactions between 5% CH_4 and N_2 in a closed system. Two experimental setups are used, where one fully removes hydrogen from the experimental system using a palladium membrane (hydrogen-poor experiments) and the other does not remove hydrogen during the experiment (hydrogen-rich experiments). Carbon isotope values ($\delta^{13}C$) of CH_4, C_2H_6, and C_3H_8 are also reported and are used, along with the gas-phase composition and relative abundance measurements, to constrain the chemical reactions occurring during our experiments. The gas-phase products C_2H_6, C_3H_8, *n*-C_4H_{10}, iso-C_4H_{10}, *n*-C_5H_{12}, iso-C_5H_{12}, C_2H_2, C_2H_4, HCN, and CH_3CN were detected, with some variations between both sets of experiments. The hydrogen-poor experiments highlight the importance of hydrogen in the formation of HCN, *n*-C_5H_{12}, iso-C_5H_{12}, and CH_3CN. By monitoring the chemical composition and the carbon isotopic ratios of the gas phase during CH_4/N_2 photochemistry, especially under a hydrogen-poor and hydrogen-rich environment, the photochemical reaction pathways and the influence of hydrogen on these pathways in a Titan-like atmosphere can be better understood.

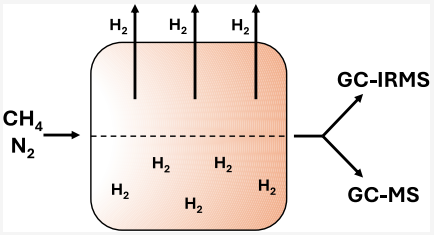

KEYWORDS: *atmospheric chemistry, gas chromatography, gases, isotopes, mass spectrometry, photochemistry*

1. INTRODUCTION

Titan's predominantly methane (CH_4) and nitrogen (N_2) atmosphere hosts complex organic chemistry resulting in the formation of organic aerosol. Numerous experimental studies over the last 40 years have simulated this chemistry in the laboratory in order to understand more about formation processes and aerosol chemical and optical properties under Titan-like atmospheric compositions.[1−15] This includes studies that have noted the influence of hydrogen on the formation of organic aerosol and the corresponding chemistry.[6,16] Excess hydrogen has been previously shown to inhibit aerosol production,[6,16] and it can also saturate the gas-phase composition.[16] As hydrogen gas is the third most abundant gas in Titan's atmosphere, understanding its influence on the photochemistry in these experiments is critical.

In addition to the importance of understanding the influence of hydrogen on the photochemical products, examining the chemical composition of the gases produced during Titan-like aerosol formation allows for reaction pathways to be elucidated. Monitoring the gas-phase composition can also provide insight into how aerosol may form in Titan's atmosphere,[15,17−24] along with a general understanding of the chemistry occurring within an experimental system and its applications to Titan's atmosphere. Furthermore, tracking the isotopic fractionation between the reactant and gas-phase products produced during photochemistry can reveal unique and complementary insight into the reaction pathways associated with aerosol formation, especially when comparing these gas-phase results to the isotopic composition of Titan-like aerosol previously studied experimentally.[25−28]

By combining gas chromatography-mass spectrometry (GC-MS) and gas chromatography-isotope ratio mass spectrometry (GC-IRMS), our experiments are the first Titan-relevant study to use stable isotopes of carbon to contextualize the gas-phase chemical composition and their corresponding changes with reaction time during far-ultraviolet (FUV) irradiation. Using a recirculating system in which CH_4 and N_2 photochemically

Received: April 17, 2024
Revised: November 25, 2024
Accepted: November 26, 2024
Published: December 5, 2024

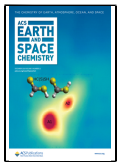

react in a closed system, our experiments operate under two conditions. The first condition is where hydrogen gas is formed via photochemistry and ultimately is allowed to build up in our system, and the second is where hydrogen gas is actively removed from the system upon its formation. These conditions allow for the comparison of both a hydrogen-rich and a hydrogen-poor scenario, which can improve our understanding of hydrogen's role in the photochemical reactions occurring within a Titan-like atmosphere in which there is some hydrogen escape. In addition, using a recirculating system and sampling at regular time intervals enables the monitoring of the gas-phase chemical composition and carbon isotopic composition of select gases as a function of reaction time, allowing for trends with time to become known.

2. EXPERIMENTAL SECTION

2.1. Recirculating System. A schematic of the recirculating system is shown in Figure 1, and during these experiments,

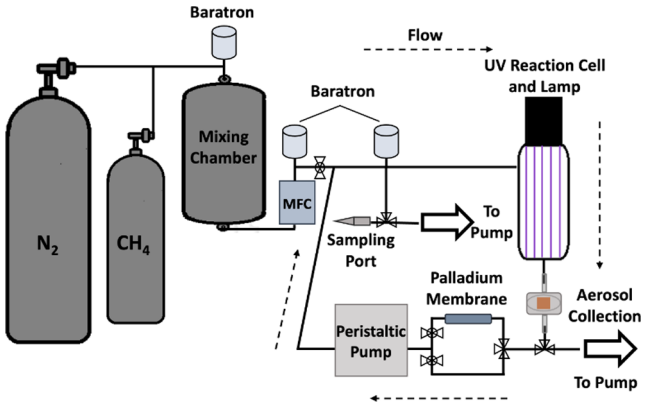

Figure 1. Schematic of the recirculating system. Gases are circulated continuously in the closed system in the direction of the dashed arrows, while aerosols are collected on a filter. The palladium membrane was used to remove hydrogen during the hydrogen-poor experiments.

no unexpected or unusually high safety hazards were encountered. The mixing chamber is connected by stainless steel tubing to the ultraviolet (UV) reaction cell inlet. On one side of the UV reaction cell, an air-cooled deuterium continuum lamp (Hamamatsu, L11798; 115−400 nm) is connected with a vacuum flange (Hamamatsu, E3444), and on the outlet of the cell, there is an aerosol collection chamber. The aerosol collection chamber is then connected to a peristaltic pump (Masterflex, L/S 07528-10P) by two pathways. The first pathway from the aerosol collection chamber to the peristaltic pump is the direct route, simply connected to the peristaltic pump via stainless steel tubing. Throughout this manuscript, the experiments performed using the first pathway are referred to as the hydrogen-rich experiments. The second pathway, prior to connecting to the peristaltic pump, first routes the gas through a custom-made, heated (200−220 °C) tubular palladium membrane that is contained within a larger stainless steel tube and held under vacuum (Power and Energy, Inc.). This system selectively passes hydrogen across the membrane, constantly removing it from our recirculating gas mixture. Since the components of the initial gas mixture and the evolved secondary gas species targeted during the study are stable at these temperatures, periodic exposure to the heated palladium membrane is not expected to influence these gases beyond removing hydrogen. Throughout this manuscript, the experiments performed using this second pathway to remove hydrogen are referred to as the hydrogen-poor experiments. Valves control which pathway is open for the gas to flow through. At the junction of the two pathways prior to entering the peristaltic pump, the stainless steel tubing is interfaced with flexible tubing (Masterflex, 06442) that is inserted into the peristaltic pump. This high-performance, chemically resistant flexible tubing is not expected to introduce loss due to absorption or adsorption, but this was not specifically investigated. The outlet of the peristaltic pump then plumbs into the inlet of the recirculating system just before the UV reaction cell. At this point, a gas sampling port is attached to enable gas extractions with gastight syringes (VICI; Series A) for measurements.

Prior to an experiment, precursor gas mixtures of 5% by volume ultrahigh purity CH_4 (Airgas, 99.99%) in ultrahigh purity N_2 (Airgas, 99.999%) are mixed for at least 8 h in the mixing chamber. Once mixed, a mass flow controller (ALICAT, MCP) flows the precursor gas mixture into the recirculating system to a pressure slightly above ambient conditions (~800 Torr, measured by a Baratron capacitance manometer; MKS, 722A). While this pressure exceeds the pressure in both Titan's upper atmosphere and stratosphere, it ensures that with gas sampling, the total pressure remains above or near ambient conditions for at least 50 h to prevent leaks into the system (see Bourgalais et al.[22] for a discussion on the challenges of performing closed-system, low-pressure, Titan-relevant experiments and the influence of chamber microleaks). After being filled, the recirculating system is isolated from the mixing chamber by a valve. To eliminate dead volume, the valve is located at the junction where the outlet of the peristaltic pump is plumbed into the recirculating system.

As the gas moves through the UV reaction cell, aerosol and gaseous photochemical products are produced. The aerosol and gas then flow to the aerosol collection chamber, where the aerosol is trapped onto a filter (Advantec/QR100 25 mm). Particles are collected rather than recirculated with the gases to prevent clogging the gastight syringes and the analyzers' inlets, along with preventing further irradiation of aerosol surfaces. The design of the recirculating system allows the precursor gas mixture and secondary gas-phase species to circulate continuously through the closed system, in the direction of the dashed arrows in Figure 1, and be exposed to the UV lamp numerous times, unlike the continuous flow system used previously where the precursor gases flow by the UV lamp only one time before analysis.[28−31] The gases are constantly recirculating during the experiment at a flow of 100 standard cubic centimeters per minute (sccm), set as the rotations per minute (rpm) by the peristaltic pump (20 rpm). This results in a residence time of about 2 min in the UV cell, and considering the total volume of the recirculating system, gases are recirculated through the UV cell about 24 times an hour.

2.2. Gas Chromatography-Mass Spectrometry. The consumption of CH_4 and the creation of secondary gas-phase products were monitored as a function of reaction time with a Thermo Scientific Trace 1310 Gas Chromatograph coupled to a Thermo Scientific ISQ QD single quadrupole mass spectrometer (GC-MS). An Rt-Q-Bond PLOT column (Restek) was used, which is optimized for hydrocarbon analysis. Using a gastight syringe, 300 μL of gas was extracted from the sampling port shown in Figure 1, and the sampled gas

https://doi.org/10.1021/acsearthspacechem.4c00102
ACS Earth Space Chem. 2024, 8, 2362−2371

was promptly injected into the GC-MS. Measurements include background gas measurements of the precursor gas mixture after flowing through the recirculating system prior to turning on the UV lamp, as well as hourly measurements of the gas mixture after turning on the UV lamp.

Mass spectra were analyzed by using Thermo Scientific XCalibur Software. To determine the retention time that corresponds to each gas, both the NIST database for electron ionization mass spectra and an alkane gas standard (Scott Gas, 303102; ±2% accuracy) were used. The gas standard contained 64% methane, 12.5% ethane, 7% propane, 3% *n*-butane, 3% iso-butane, 0.5% *n*-pentane, 0.5% iso-pentane, 0.5% carbon dioxide, and 9% nitrogen and was needed to determine the retention times of isomers. Due to the difficulties in obtaining a nitrile standard, only a hydrocarbon standard was used in these experiments.

2.3. Gas Chromatography-Isotope Ratio Mass Spectrometry. The carbon isotope ratios of CH_4, C_2H_6, and C_3H_8 were measured using a Thermo Scientific Trace Ultra Gas Chromatograph IsoLink with a Carboxen 1006 PLOT column (Supelco) coupled through an oxidation reactor to a Thermo Scientific Delta V Isotope Ratio Mass Spectrometer (GC-IRMS). CH_4 was measured separately from C_2H_6 and C_3H_8 because of their differences in concentration. 100 μL was extracted for the CH_4 analysis, and then 500 μL was extracted for the C_2H_6 and C_3H_8 analysis. To ensure there was no pressure-dependent fractionation occurring due to our methodology of sequential extractions, we performed a study where the precursor gas mixture recirculated in the system with the lamp off for over 5 h. Sequential extractions were removed hourly, and there was no trend in the $\delta^{13}C$ of the CH_4. This indicates that our sampling method does not introduce any pressure-dependent fractionation that could bias our results.

After the GC column separates the injected gas species, they are combusted on an oxidation reactor, and the resulting CO_2 is analyzed on the IRMS using Thermo Scientific Isodat Software. The IRMS is designed for stable isotope measurements and determines small changes in carbon isotope ratios. Here, the carbon isotope ratio, $\delta^{13}C$, is reported in per mil (‰) relative to Vienna Pee Dee Belemnite (VPDB) as follows

$$\delta^{13}C = \left(\frac{^{13}C/^{12}C_{sample}}{^{13}C/^{12}C_{VPDB}} - 1 \right) \times 1000 \quad (1)$$

Furthermore, the difference in $\delta^{13}C$ values of the products relative to the precursor CH_4 is defined as $\Delta^{13}C$ where

$$\Delta^{13}C = \delta^{13}C_{products} - \delta^{13}C_{CH_4,t=0} \quad (2)$$

When $\Delta^{13}C$ is positive, the product is enriched in ^{13}C relative to the starting CH_4, and when $\Delta^{13}C$ is negative, the product is depleted in ^{13}C relative to the starting CH_4.

Once the initial gas mixture was introduced into the recirculating system, the isotopic composition of the reactant CH_4 was measured following the peristaltic pump being switched on but before the UV lamp was turned on. This initial CH_4 was measured at least three times prior to the onset of photolysis to ensure precision in the starting $\delta^{13}C$, and the average standard deviation of these starting CH_4 $\delta^{13}C$ measurements was 0.20‰. By adjusting for the initial CH_4 of each individual run, we corrected for any differences in fractionation that occurred prior to the introduction of the gas into the recirculating system. Once the UV lamp was turned on, GC-IRMS measurements were performed hourly, offset by 30 min from the GC-MS measurements.

3. RESULTS AND DISCUSSION

3.1. Gas Chemical Composition. The consumption of CH_4 and the evolution of the secondary products were characterized by GC-MS. Table 1 lists the compounds

Table 1. Photochemical Products Characterized by GC-MS during the Hydrogen-Rich and Hydrogen-Poor Experiments[a]

compound	hydrogen-rich	hydrogen-poor	(6 h)	(24 h)
C_2H_2	√	√	(+)	(+)
C_2H_4	√	√	(+)	(+)
C_2H_6	√	√	(−)	(+)
C_3H_8	√	√	(−)	(+)
n-C_4H_{10}	√	√	(−)	(+)
iso-C_4H_{10}	√	√	(−)	(+)
n-C_5H_{12}	√	×	×	×
iso-C_5H_{12}	√	×	×	×
HCN	√	×	×	×
CH_3CN	√	√	(−)	(−)

[a]For products detected in both experiments, (+) and (−) indicate if more or less of that product was detected in the hydrogen-poor experiments compared to that in the hydrogen-rich experiments at hour 6 and hour 24.

detected during the hydrogen-rich and hydrogen-poor experiments, and whether more (+) or less (−) of each compound was measured in the hydrogen-poor experiments compared to that in the hydrogen-rich experiments at two time points (6 and 24 h) is included as well. Between both experiments, the photochemical products identified include C_2H_6, C_3H_8, *n*-C_4H_{10}, iso-C_4H_{10}, *n*-C_5H_{12}, iso-C_5H_{12}, C_2H_2, C_2H_4, HCN, and CH_3CN, with some specific variations between the type of experiment. First, the hydrogen-poor experiments did not result in the production of HCN, *n*-C_5H_{12}, or iso-C_5H_{12}, highlighting the importance of H_2 (and H radicals) in the formation of these products. The absence of HCN in the hydrogen-poor experiments supports its recently modeled formation pathways.[32] Here, the formation of HCN in Titan's atmosphere is proposed to predominantly stem from three different pathways, all of which include the reaction of the intermediate byproduct H_2CN with either a hydrogen radical or a hydrogen radical and hydrogen gas

$$H_2CN + H_2 + H \rightarrow HCN + 2H_2 \quad (R1)$$

$$H_2CN + H \rightarrow HCN + H_2 \quad (R2)$$

H can result from the numerous reaction pathways and photolysis undergone by CH_4, CH_3, CH_2, and other hydrocarbons and hydrogen-containing compounds.[32−36] Following its formation, the reaction $2H + N_2 \rightarrow H_2$ is likely happening preferentially in our system given the high pressure of N_2 in our mixtures.[32] The removal of H_2 by the hydrogen purifier then results in the lack of detected HCN in these experiments since there would be no H_2 (R1) and no H radicals (R1, R2) resupplied to the system from the photolysis of H_2 to react with H_2CN when the gas mixture is recirculated by the UV lamp. However, because the gases flow through the UV reaction cell prior to passing through the hydrogen purifier, it is likely that some HCN is forming in our system

https://doi.org/10.1021/acsearthspacechem.4c00102
ACS Earth Space Chem. 2024, 8, 2362−2371

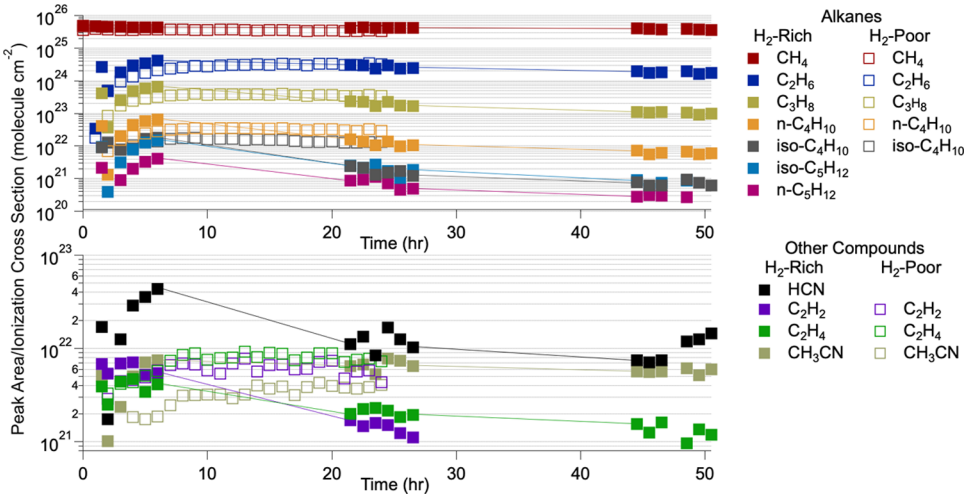

Figure 2. Peak areas of each detected compound normalized to their electron ionization cross section at 70 eV as a function of the reaction time. Solid squares correspond to hydrogen-rich experiments, and open squares correspond to hydrogen-poor experiments. Alkanes are in the top panel, and the other compounds characterized during these experiments are in the bottom panel. The ionization cross section of *n*-C_5H_{12} was used for iso-C_5H_{12} as there is no reported electron ionization cross section for iso-C_5H_{12}.

during the hydrogen-poor experiments, albeit below the detection limit of the GC-MS.

As for iso-C_5H_{12} and *n*-C_5H_{12}, while neither of these compounds have been observed in Titan's atmosphere (in addition to iso-C_4H_{10} and *n*-C_4H_{10}), *n*-C_5H_{12} has been detected in numerous other Titan-relevant photochemical aerosol generation experiments,[17,37,38] whereas iso-C_5H_{12} has been detected in only one other photochemical aerosol generation experiment.[39] The photochemical formation pathways responsible for the formation of *n*-C_5H_{12} and iso-C_5H_{12} have been unexplored in these experimental studies, in addition to photochemical modeling studies, perhaps since a C_5-saturated hydrocarbon is unlikely to participate in the formation of aerosol.[40−44] Even so, it is possible C_5H_{12} forms by a similar reaction pathway as C_4H_{10}.[36] C_4H_{10} is formed in two steps, involving the intermediate C_3H_7

$$H + C_3H_6 \xrightarrow{M} C_3H_7 \quad \text{(R3)}$$

$$C_3H_7 + CH_3 \xrightarrow{M} C_4H_{10} \quad \text{(R4)}$$

It is possible the same could happen for C_5H_{12} where the intermediate C_4H_9 first forms and then reacts with CH_3 to form C_5H_{12}. As the first step in this speculative reaction pathway would require H, this would explain why no C_5H_{12} is observed in the hydrogen-poor experiments, and it also suggests there are non-hydrogen required pathways that can produce C_4H_{10} but not C_5H_{12} (or at least not in quantities above our detection limit). However, to be certain of this, further photochemical modeling must be performed.

There are two other closed-system studies that used similar wavelengths to initiate photochemistry that we can compare our results with.[37,38] In these experiments, CH_4 and N_2 with and without helium gas were irradiated in a closed system by the sun ($\lambda \geq 115$ nm due to the use of a MgF_2 window, similar to that used on the UV lamp in our experimental setup) while they were positioned outside the International Space Station (ISS). Both studies used a larger percentage of CH_4 compared to that of N_2 than found in Titan's atmosphere, with 50% CH_4[37] and 62.5% CH_4[38] being used. Using GC-MS, the photolysis products C_2H_6, C_3H_8, *n*-C_4H_{10}, iso-C_4H_{10}, and *n*-C_5H_{12} were identified upon the samples' return to Earth. The lack of unsaturated hydrocarbons was explained as being due to the larger total pressure of the gas mixtures (1125 Torr),[38] and while nitrogen was found to be incorporated into the solid phase, the lack of nitrogen-containing gaseous products was not explained. As we identify nitriles in the current study under both experimental conditions, it is possible that the larger percentage of CH_4 compared to that of N_2 in the ISS studies could explain the lack of nitrile species. This phenomenon is supported in the literature, where using increasing amounts of CH_4 to photochemically produce aerosol in a continuous flow system decreases the abundances of nitrile photochemical products.[20] In addition, large percentages of CH_4 compared to those of the other gases in a gas mixture have been shown to inhibit the formation of intermediate products by shielding the other gases from UV photons.[10] Since the ISS experiment was not performed in a continuous flow or in a recirculating closed system, the shielding of photons by CH_4 could have been exacerbated and influenced the measured gas-phase products, possibly resulting in the lack of unsaturated hydrocarbons and nitriles as well. It is important to note here that while $\lambda \geq 115$ nm is insufficient to break the N_2 triple bond, nitrogen chemistry has been observed in numerous photochemical experiments with this insufficient energy, including the current study, but the chemical pathways resulting in this are still not known.[3,11,12,14,15,20,28,31,38,45−54]

3.2. Gas Relative Abundance. In addition to compositional distinctions between the two experimental methods, there are also gas abundance differences, although the reported amounts of gaseous products with lower volatility, i.e., *n*-C_5H_{12} and iso-C_5H_{12}, are likely less than what is actually produced during these experiments due to losses to the chamber walls. The gas abundance differences are most noticeable when the experiments are compared as a function of time. For the hydrogen-rich experiments, following a rapid increase in the production of higher-order gas species, there is a decline in those abundances, which then somewhat level off after about 44 h. Alternatively, for the hydrogen-poor experiments, following the increase in the production of the different gases, the product abundances appear to eventually reach a steady state within 24 h and do not decline with time as

https://doi.org/10.1021/acsearthspacechem.4c00102
ACS Earth Space Chem. 2024, 8, 2362−2371

observed during the hydrogen-rich experiments. Since the secondary products reach a steady state around hour 8, the hydrogen-poor experiments were not extended beyond 24 h like the hydrogen-rich experiments. In both scenarios, the variation in the abundance with time is closely tied to the presence or lack of hydrogen. When hydrogen is removed, the gases continue to react and form more photochemical products each time they flow by the UV lamp. When hydrogen is not removed, it builds up in the system and inhibits reactions that form larger products from occurring. The amount of hydrogen produced during our hydrogen-rich studies is about 1% by volume by the end of the experiment, which is enough to influence the chemistry observed in these recirculating, closed-system experiments. This concentration was determined based on pressure readings by a pressure transducer sensitive to gas thermal conductivity used during a subset of these experiments (substituted for the Baratron shown in Figure 1 before the sampling port) and is comparable with the amount of H_2 measured by Cassini CIRS[55,56] and Huygens GC-MS[57] in Titan's troposphere.

In order to quantitatively compare the peak areas of the characterized compounds to each other, their ionization cross sections must be considered since different compounds will ionize more readily than others. Figure 2 compares the relative abundance of each compound measured during hydrogen-poor (open squares) and hydrogen-rich (closed squares) experiments by normalizing the GC-measured peak areas of each compound to their corresponding ionization cross section at 70 eV (energy of the MS electron ionization source).[58−65] There are small discrepancies between theoretically and experimentally determined electron ionization cross sections, but using either result in only minor changes in their normalized peak areas. Even so, experimental ionization cross sections were used in all cases except iso-C_4H_{10}, which only had a theoretical ionization cross section available. In addition, as there is no reported electron ionization cross section for iso-C_5H_{12}, the ionization cross section for n-C_5H_{12} was used. A summary of the relative difference per compound is included in Table 1 at hours 6 and 24. For compounds that were detected in both experiments, the symbols (+) and (−) denote whether more or less, respectively, of that compound was detected in the hydrogen-poor experiments compared to that in the hydrogen-rich experiments.

Initially (hour 6), C_2−C_4 alkanes were produced in less abundance during the hydrogen-poor experiments, but by the end of the hydrogen-poor studies (hour 24), these alkanes were then synthesized in more abundance during these experiments compared to the hydrogen-rich experiments. This trend is consistent with the hydrogen-rich experiments becoming saturated, resulting in fewer products forming over time. For both C_2H_2 and C_2H_4, more is produced in the hydrogen-poor experiments at both 6 and 24 h. However, prior to hour 5, C_2H_2 and C_2H_4 are formed in lower amounts during the hydrogen-poor experiments than during the hydrogen-rich experiments, where hydrogen saturation appears to influence the fate of these compounds sooner than that of the alkanes. A possible explanation for this is that in the presence of large amounts of hydrogen, C_2H_4 may undergo a series of reactions where the net reaction is its reaction with H radicals to form C_2H_6 (R5).[33] Additionally, C_2H_2 may react with H radicals to form C_2H_3 (R6),[33,66] which can further react with H_2 to make C_2H_4 (R7)[33,66] and then ultimately C_2H_6 by R5

$$C_2H_4 + 2H \rightarrow C_2H_6 \quad \text{(R5)}$$

$$C_2H_2 + H \xrightarrow{M} C_2H_3 \quad \text{(R6)}$$

$$C_2H_3 + H_2 \rightarrow C_2H_4 + H \quad \text{(R7)}$$

As for the other secondary gas products, once these gases start declining in abundance during the hydrogen-rich experiments, it is due to back reactions forming CH_4. A likely reaction that could be ongoing during the hydrogen-rich experiments due to the larger H_2 mixing ratio includes the reaction of CH_3 with H_2 forming CH_4 (R8),[66] which could be occurring preferentially to the reaction of CH_3 forming C_2H_6 (R9)[33,66] or C_2H_4 (R10)[36]

$$H_2 + CH_3 \rightarrow CH_4 + H \quad \text{(R8)}$$

$$2CH_3 \xrightarrow{M} C_2H_6 \quad \text{(R9)}$$

$$^3CH_2 + CH_3 \rightarrow C_2H_4 + H \quad \text{(R10)}$$

The preference of R8 to R10 during the hydrogen-rich experiments could also contribute to the decrease in the relative amount of C_2H_2 during these experiments as well since one of the main pathways of its formation is from the photolysis of C_2H_4.[33]

Other reactions that are likely occurring during the hydrogen-rich experiments that could also explain the change in relative abundance of the other hydrocarbons include the following loss mechanism of C_2H_4 that ultimately results in the back reaction to CH_4[66]

$$C_2H_4 + H \xrightarrow{M} C_2H_5 \quad \text{(R11)}$$

$$C_2H_5 + H \rightarrow 2CH_3 \quad \text{(R12)}$$

$$H_2 + CH_3 \rightarrow CH_4 + H \quad \text{(R13)}$$

Similar reaction pathways back to CH_4 with the other hydrocarbons produced in our studies could be occurring as well to explain the decrease in production with reaction time. This includes the loss of C_2H_6 through the formation of C_2H_5 ($H + C_2H_6 \rightarrow C_2H_5 + H_2$),[66] which then would back react to form CH_4 via R12 and R13.

Possibly the most notable distinction between the relative abundances of each gas produced in both types of experiments is the amount of CH_3CN. CH_3CN is produced in lower relative abundance during hydrogen-poor experiments compared with that of hydrogen-rich experiments at all times. Furthermore, CH_3CN is synthesized in the lowest relative abundance in the hydrogen-poor experiments compared with the rest of the gaseous products in those experiments, which is not the case during the hydrogen-rich experiments. During the hydrogen-rich experiments, while CH_3CN is one of the more trace gaseous products, it is still made in relatively more abundance than the other nonalkanes and n-C_5H_{12} during the full experiment and in more abundance than iso-C_4H_{10} and iso-C_5H_{12} by hour 21.5. This again is likely due to the role of hydrogen in the reaction pathway to CH_3CN, which forms by reactions of C_2H_4 (R14)[36,43,67] and C_2H_3 (R15)[43,68] with N (see Section 3.1 regarding nitrogen chemistry during these experiments), where

$$C_2H_4 + N(^2D) \rightarrow CH_3CN + H \quad \text{(R14)}$$

$$C_2H_3 + N(^4S) \rightarrow CH_3CN \quad \text{(R15)}$$

https://doi.org/10.1021/acsearthspacechem.4c00102
ACS Earth Space Chem. 2024, 8, 2362−2371

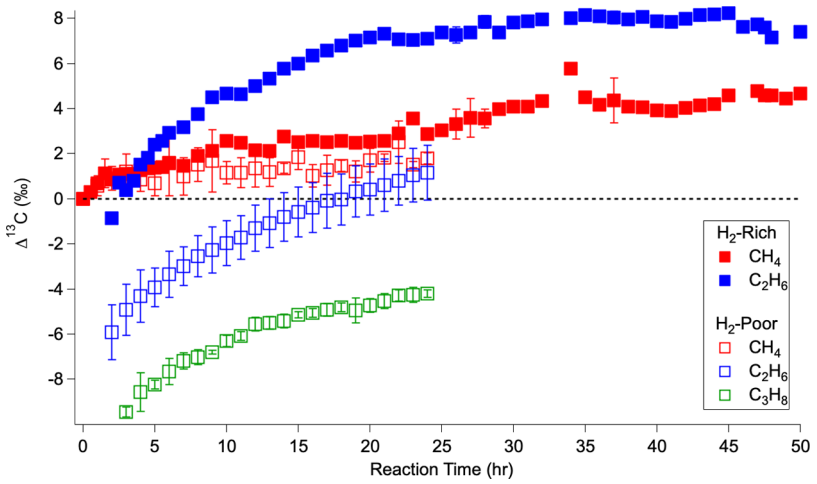

Figure 3. Temporal evolution of carbon isotope ratios of the sufficiently abundant alkanes over the course of the hydrogen-rich experiments (solid squares) and the hydrogen-poor experiments (open squares). These ratios are presented as $\Delta^{13}C$, which is the difference between the measured $\delta^{13}C$ of a given compound at a given time and the $\delta^{13}C$ of the initial CH_4 for each run (eq 2). Error bars are the standard deviation for the experiments averaged into each time point.

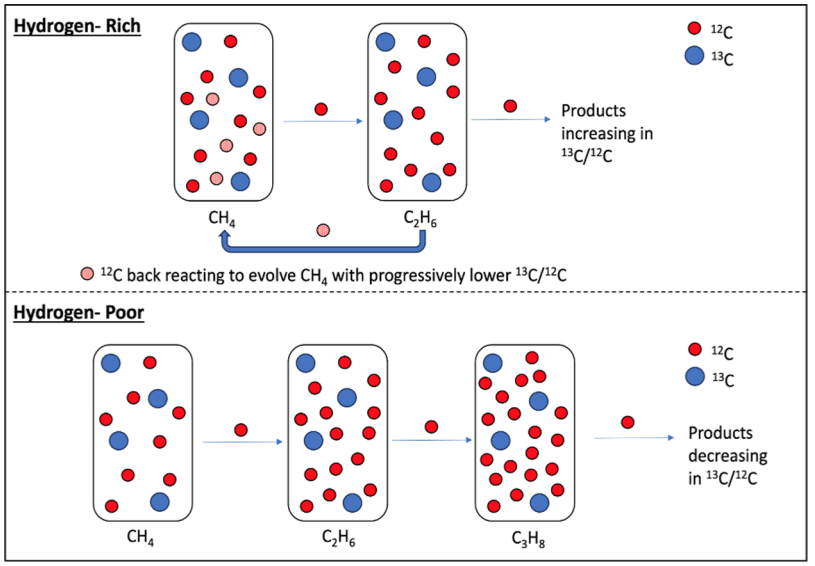

Figure 4. Summary of the isotopic evolution of the gases produced in sufficient abundance for GC-IRMS measurements during the hydrogen-rich (top panel) and hydrogen-poor (bottom panel) experiments.

The fact that the relative amount of C_2H_4 compared to the other minor products is the same between experiment types (with the exception when compared to CH_3CN) points to C_2H_3 concentration changes being at play. C_2H_3 can form either via C_2H_2 (R6)[69] or C_2H_4 (R16)[70]

$$C_2H_4 + H \rightarrow C_2H_3 + H_2 \quad \text{(R16)}$$

As these reactions rely on H, the decreased relative abundance of CH_3CN in the hydrogen-poor experiments can be explained by one of its required intermediates (C_2H_3) being produced in a lower abundance than in the hydrogen-rich experiments.

No experimental setup can truly reproduce Titan's atmosphere. Even so, experimental simulations of Titan's atmospheric chemistry can provide insight into the processes occurring in the atmosphere and the factors that control those processes, thus providing support to the conclusions drawn from observational and modeling studies. Due to experimental constraints in the current study, the pressure in our system is greater than the pressure in Titan's upper atmosphere and stratosphere. In addition, gases in these studies are exposed to a greater photon flux at Lyman-α from the UV lamp (about 4 orders of magnitude greater) than the gases in Titan's upper atmosphere.[10,50] The pressure of the gas mixture influences reaction kinetics and the abundance of the gaseous products, as does the greater photon flux, and so while the products formed during our experiments are relevant for Titan's atmosphere, their abundances are likely unique to our system. Even so, CH_4 and the secondary gases measured in the current study all strongly absorb across the UV lamp's wavelength range,[71−82] highlighting the relevance of the photochemistry occurring in this study to that in Titan's atmosphere. Similarly, it is therefore difficult to directly compare the concentration of gases measured in this study to any previous Titan-relevant studies due to differences in experimental setups (including energy sources, pressure, temperature, etc.) and analytical techniques.[15,20] However, the gas-phase species measured in

https://doi.org/10.1021/acsearthspacechem.4c00102
ACS Earth Space Chem. 2024, 8, 2362−2371

this study have been previously observed in other Titan photochemical aerosol studies to various degrees.[3,15,20,37−39,83] Of these studies, two also used the same energy source as the present study.[15,20] Due to the soft ionization techniques used by the mass spectrometers in these two previous studies, comparing with the results of the current study is challenging, since compounds with lower proton affinities could not be measured by their instruments. In addition, Berry et al.[15] state that quantifying the compounds measured during their studies was not possible due to the compound signals being uncalibrated. So, while there are studies with fewer variables that differ from the present study, conclusions from a comparison between these three studies are still not possible.

3.3. Alkane Carbon Isotopic Composition. The isotope ratios of the alkanes that were produced in sufficient abundance for GC-IRMS measurements are shown in Figure 3, and there are significant differences between the two types of experiments performed. A dashed line at $\Delta = 0$ has been added to aid in viewing the gas species enriched (>0) and depleted (<0) in ^{13}C relative to the starting CH_4. The carbon isotope ratios of CH_4 and C_2H_6 were measured during the hydrogen-rich experiments, and the carbon isotope ratios of CH_4, C_2H_6, and C_3H_8 were measured during the hydrogen-poor experiments. During the hydrogen-rich experiments (solid squares), CH_4 becomes isotopically enriched relative to its starting composition and continues to grow heavier across the entire evolution of the system. While C_2H_6 is initially isotopically depleted relative to the starting CH_4—as expected from kinetically driven processes since the lighter isotopes react faster and more often than the heavier isotopes—it then rapidly becomes enriched relative to the starting CH_4 and eventually becomes enriched relative to the CH_4 in the system at the same time. The evolution of the isotopic measurements during the hydrogen-rich experiments supports the reaction pathways described in Section 3.2 for the hydrogen-rich experiments, where, as photochemistry progresses, H_2 builds up and back reactions toward CH_4 dominate the system. As depicted in the top panel of Figure 4, since the $^{13}C-^{12}C$ bond is harder to break, the $^{12}C-^{12}C$ bond of C_2H_6 is preferentially photolyzed and reacted back to $^{12}CH_4$, causing the enrichment of C_2H_6 relative to the contemporaneous CH_4. This represents an equilibrium-dominated regime in which the isotopic composition of the atmospheric gases is driven by bond stability.

Alternatively, for the hydrogen-poor experiments (open squares), Figure 3 portrays a different reaction pathway for these studies, with only some similarities to the hydrogen-rich experiments. Like the hydrogen-rich experiments, during the hydrogen-poor experiments, CH_4 becomes enriched relative to its starting composition. And again, the earliest C_2H_6 is depleted relative to the starting CH_4; however, it is depleted by a significantly larger amount than in the hydrogen-rich experiments. Then, over time, C_2H_6 becomes enriched and approaches the isotopic composition of the simultaneous CH_4, but unlike the hydrogen-rich experiments, it does not surpass it. During the hydrogen-poor experiments, enough C_3H_8 is produced for isotopic measurements, and it is yet further depleted relative to the C_2H_6 and starting CH_4, and has a similar isotopic evolution to C_2H_6 over the course of the experiment. These isotopic measurements, as summarized in the bottom panel of Figure 4, also support the reaction pathways described in the previous subsections that highlight the importance of hydrogen. Specifically, the consistent depletion across each higher-order hydrocarbon follows expectations for $\delta^{13}C$ in a kinetically dominated reaction system. Thus, the hydrogen-poor experiments represent a kinetically driven regime where the isotopic composition and makeup of atmospheric gases are driven by unidirectional forward photochemical reactions.

3.3.1. Comparison to Experimental Isotope Ratios of Photochemical Aerosol. Previous work determined the carbon isotope ratios of photochemical aerosol produced with varying amounts of CH_4 in N_2 in a continuous flow system.[28] While the extent of isotopic fractionation varied, each scenario resulted in photochemical aerosol that was enriched in ^{13}C. This is opposite of the kinetic isotope effect, which is what was expected for photochemically formed aerosol, and the possible causes of this enrichment in ^{13}C was discussed.[28] While the carbon isotopic ratio of the aerosol and initial reactant CH_4 was reported for these aerosol studies, the isotopic ratio of the gas-phase products and unreacted CH_4 was not measured. Without this information, it is unknown as to why photochemical aerosol would be enriched rather than depleted in ^{13}C.

The recirculating experiments in the current study provide a way to monitor the gas-phase products and unreacted CH_4; however, the experimental methods of the recirculating system are not directly comparable to the continuous flow system experiments. Specifically, a continuous flow system represents an open system in which reactants are continuously supplied, while in a recirculating system, reactants can be depleted by the formation of products and back reactions can occur. In the recirculating system, the gases are exposed to the UV lamp for a total of 48 min every hour and in the continuous flow system, the gases are exposed to the UV lamp for 2 min in total. Even so, the closest comparison we can make between the recirculating experiments and the continuous flow system experiments is at the earliest time points in the time series. In the current study, by hour 2, there was sufficient signal for ^{13}C measurements of C_2H_6, and by hour 3, there was sufficient signal for ^{13}C measurements of C_3H_8. For both experiments, hydrogen-rich and hydrogen-poor, the C_2H_6 produced by hour 2 was depleted compared to the concurrent CH_4. The same is true for C_3H_8 during the hydrogen-poor experiments that were first measured at hour 3: C_3H_8 was depleted compared to the concurrent C_2H_6 and CH_4. The photochemically produced species being depleted in ^{13}C compared to the initial and unreacted CH_4 is expected. The primary photochemical products of CH_4 photolysis following the kinetic isotope effect have further implications on why the photochemically produced aerosol is instead enriched in ^{13}C. Specifically, higher-order reactions with more complex organic compounds that are responsible for aerosol formation could result from reactions that preferentially proceed with the heavier carbon isotope, resulting in the aerosol formed to also be enriched as well.[28] Further isotope measurements of these higher-order complex organic species are needed in order to resolve the question of why the experimentally formed photochemical aerosol is enriched in ^{13}C, but accumulating enough of these complex organic species for measurements remains a challenge.

4. CONCLUSIONS

The time-dependent chemical composition characterized by GC-MS of the photochemical gas-phase products produced from FUV irradiation of 5% CH_4 in N_2 in a closed system under hydrogen-rich and hydrogen-poor conditions is

https://doi.org/10.1021/acsearthspacechem.4c00102
ACS Earth Space Chem. 2024, 8, 2362−2371

reported. The reaction pathways forming these gases are discussed and further contextualized with $\delta^{13}C$ isotopic measurements of CH_4, C_2H_6, and C_3H_8 as functions of reaction time. Between the hydrogen-poor and hydrogen-rich experiments, C_2H_6, C_3H_8, n-C_4H_{10}, iso-C_4H_{10}, n-C_5H_{12}, iso-C_5H_{12}, C_2H_2, C_2H_4, HCN, and CH_3CN were detected as gas-phase products. The hydrogen-poor experiments highlight the importance of hydrogen in the formation of HCN, n-C_5H_{12}, and iso-C_5H_{12}. Furthermore, the presence of hydrogen also appears to greatly influence the relative amount of CH_3CN that can photochemically form in a Titan-like system. Lastly, the isotopic evolution of CH_4, C_2H_6, and for the hydrogen-poor experiment, C_3H_8, demonstrates the direction of the reactions in each experimental system toward products versus a back reaction to CH_4 related to the abundance of hydrogen. By monitoring the gas-phase chemical composition and isotopic fractionation during laboratory Titan-like atmospheric photochemical simulations, these experiments not only provide insight into the chemical processes occurring in our experiments but also provide insight into reaction pathways that could be occurring in Titan's atmosphere and the role of hydrogen on these reaction pathways.

AUTHOR INFORMATION

Corresponding Author

Melissa S. Ugelow − *NASA Goddard Space Flight Center, Greenbelt, Maryland 20771, United States;* orcid.org/0000-0001-9725-6624; Email: melissa.ugelow@nasa.gov

Authors

Scott T. Wieman − *Department of Geology and Geophysics, Woods Hole Oceanographic Institution, Woods Hole, Massachusetts 02543, United States; Department of Earth, Atmospheric, and Planetary Sciences, Massachusetts Institute of Technology, Cambridge, Massachusetts 02139, United States;* orcid.org/0000-0002-6415-5293

Madeline C. R. Schwarz − *Department of Chemistry, Colorado State University, Fort Collins, Colorado 80523, United States;* orcid.org/0000-0002-0373-5788

Victoria Da Poian − *NASA Goddard Space Flight Center, Greenbelt, Maryland 20771, United States; Microtel LLC, Greenbelt, Maryland 20771, United States; Johns Hopkins University, Baltimore, Maryland 21218, United States*

Jennifer C. Stern − *NASA Goddard Space Flight Center, Greenbelt, Maryland 20771, United States*

Melissa G. Trainer − *NASA Goddard Space Flight Center, Greenbelt, Maryland 20771, United States*

Complete contact information is available at: https://pubs.acs.org/10.1021/acsearthspacechem.4c00102

Notes

The authors declare no competing financial interest.

ACKNOWLEDGMENTS

This research was supported by the NASA Planetary Science Division Internal Scientist Funding Program through the Fundamental Laboratory Research (FLaRe) work package.

REFERENCES

(1) Khare, B.; Sagan, C.; Thompson, W. R.; Arakawa, E. T.; Suits, F.; Callcott, T. A.; Williams, M. W.; Shrader, S.; Ogino, H.; Willingham, T.; Nagy, B. The organic aerosols of Titan. *Adv. Space Res.* **1984**, *4*, 59−68.

(2) Khare, B.; Sagan, C.; Arakawa, E.; Suits, F.; Callcott, T.; Williams, M. Optical constants of organic tholins produced in a simulated Titanian atmosphere: From soft x-ray to microwave frequencies. *Icarus* **1984**, *60*, 127−137.

(3) Scattergood, T. W.; McKay, C. P.; Borucki, W. J.; Giver, L. P.; van Ghyseghem, H.; Parris, J. E.; Miller, S. L. Production of organic compounds in plasmas: A comparison among electric sparks, laser-induced plasmas, and UV light. *Icarus* **1989**, *81*, 413−428.

(4) McKay, C. P. Elemental composition, solubility, and optical properties of Titan's organic haze. *Planet. Space Sci.* **1996**, *44*, 741−747.

(5) Ramirez, S.; Coll, P.; da Silva, A.; Navarro-González, R.; Lafait, J.; Raulin, F. Complex Refractive Index of Titan's Aerosol Analogues in the 200−900 nm Domain. *Icarus* **2002**, *156*, 515−529.

(6) Sciamma-O'Brien, E.; Carrasco, N.; Szopa, C.; Buch, A.; Cernogora, G. Titan's atmosphere: An optimal gas mixture for aerosol production? *Icarus* **2010**, *209*, 704−714.

(7) Sciamma-O'Brien, E.; Dahoo, P. R.; Hadamcik, E.; Carrasco, N.; Quirico, E.; Szopa, C.; Cernogora, G. Optical constants from 370 to 900 nm of Titan tholins produced in a low pressure RF plasma discharge. *Icarus* **2012**, *218*, 356−363.

(8) Mahjoub, A.; Carrasco, N.; Dahoo, P.; Gautier, T.; Szopa, C.; Cernogora, G. Influence of methane concentration on the optical indices of Titan's aerosols analogues. *Icarus* **2012**, *221*, 670−677.

(9) Trainer, M. G.; Pavlov, A.; Jimenez, J.; McKay, C.; Worsnop, D.; Toon, O.; Tolbert, M. Chemical composition of Titan's haze: Are PAHs present? *Geophys. Res. Lett.* **2004**, *31*, No. L17S08.

(10) Trainer, M. G.; Pavlov, A.; DeWitt, H.; Jimenez, J.; McKay, C.; Toon, O.; Tolbert, M. Organic haze on Titan and the early Earth. *Proc. Natl. Acad. Sci. U.S.A.* **2006**, *103*, 18035−18042.

(11) Trainer, M. G.; Jimenez, J.; Yung, Y.; Toon, O.; Tolbert, M. Nitrogen Incorporation in CH_4-N_2 Photochemical Aerosol Produced by Far Ultraviolet Irradiation. *Astrobiology* **2012**, *12*, 315−326.

(12) Trainer, M. G.; Sebree, J.; Yoon, Y.; Tolbert, M. THE INFLUENCE OF BENZENE AS A TRACE REACTANT IN TITAN AEROSOL ANALOGS. *Astrophys. J. Lett.* **2013**, *766*, No. L4.

(13) Cable, M. L.; Horst, S.; Hodyss, R.; Beauchamp, P.; Smith, M.; Willis, P. Titan tholins: simulating Titan organic chemistry in the Cassini-Huygens era. *Chem. Rev.* **2012**, *112*, 1882−909.

(14) Berry, J. L.; Ugelow, M. S.; Tolbert, M. A.; Browne, E. C. Chemical Composition of Gas-Phase Positive Ions during Laboratory Simulations of Titan's Haze Formation. *ACS Earth Space Chem.* **2019**, *3*, 202−211.

(15) Berry, J. L.; Ugelow, M. S.; Tolbert, M. A.; Browne, E. C. The Influence of Gas-phase Chemistry on Organic Haze Formation. *Astrophys. J. Lett.* **2019**, *885*, L6.

(16) DeWitt, H. L.; Trainer, M. G.; Pavlov, A. A.; Hasenkopf, C. A.; Aiken, A. C.; Jimenez, J. L.; McKay, C. P.; Toon, O. B.; Tolbert, M. A. Reduction in Haze Formation Rate on Prebiotic Earth in the Presence of Hydrogen. *Astrobiology* **2009**, *9*, 447−453.

(17) Imanaka, H.; Smith, M. A. From the Cover: Formation of nitrogenated organic aerosols in the Titan upper atmosphere. *Proc. Natl. Acad. Sci. U.S.A.* **2010**, *107*, 12423−12428.

(18) Carrasco, N.; Gautier, T.; Es-sebbar, E.-t.; Pernot, P.; Cernogora, G. Volatile products controlling Titan's tholins production. *Icarus* **2012**, *219*, 230−240.

(19) Gautier, T.; Carrasco, N.; Stefanovic, I.; Sikimic, B.; Cernogora, G.; Winter, J. Methane Conversion in a N_2−CH_4 Radiofrequency Discharge. *Plasma Processes Polym.* **2014**, *11*, 472−481.

(20) Hörst, S. M.; Yoon, Y. H.; Ugelow, M. S.; Parker, A. H.; Li, R.; de Gouw, J. A.; Tolbert, M. A. Laboratory investigations of Titan haze formation: In situ measurement of gas and particle composition. *Icarus* **2018**, *301*, 136−151.

(21) Dubois, D.; Carrasco, N.; Petrucciani, M.; Vettier, L.; Tigrine, S.; Pernot, P. In situ investigation of neutrals involved in the formation of Titan tholins. *Icaurs* **2019**, *317*, 182−196.

(22) Bourgalais, J.; Carrasco, N.; Vettier, L.; Gautier, T.; Blanchet, V.; Petit, S.; Descamps, D.; Fedorov, N.; Delos, R.; Gaudin, J. On an

EUV Atmospheric Simulation Chamber to Study the Photochemical Processes of Titan's Atmosphere. *Sci. Rep.* **2020**, *10*, No. 10009.
(23) Chudják, S.; Kozáková, Z.; Krčma, F. Study of Chemical Processes Initiated by Electrical Discharge in Titan-Related Atmosphere at Laboratory Temperature and Pressure. *ACS Earth Space Chem.* **2021**, *5*, 535−543.
(24) He, C.; Serigano, J.; Hörst, S. M.; Radke, M.; Sebree, J. A. Titan Atmospheric Chemistry Revealed by Low-Temperature N2−CH4 Plasma Discharge Experiments. *ACS Earth Space Chem.* **2022**, *6*, 2295−2304.
(25) Kuga, M.; Carrasco, N.; Marty, B.; Marrocchi, Y.; Bernard, S.; Rigaudier, T.; Fleury, B.; Tissandier, L. Nitrogen isotopic fractionation during abiotic synthesis of organic solid particles. *Earth Planet. Sci. Lett.* **2014**, *393*, 2−13.
(26) Nguyen, M. J.; Raulin, F.; Coll, P.; Derenne, S.; Szopa, C.; Cernogora, G.; Israël, G.; Bernard, J. M. Carbon isotopic enrichment in Titan's tholins? Implications for Titan's aerosols. *Planet. Space Sci.* **2007**, *55*, 2010−2014.
(27) Nguyen, M.-J.; Raulin, F.; Coll, P.; Derenne, S.; Szopa, C.; Cernogora, G.; Israël, G.; Bernard, J.-M. From Titan's tholins to Titan's aerosols: Isotopic study and chemical evolution at Titan's surface. *Adv. Space Res.* **2008**, *42*, 48−53.
(28) Sebree, J. A.; Stern, J. C.; Mandt, K. E.; Domagal-Goldman, S. D.; Trainer, M. G. ^{13}C and $^{1}5N$ fractionation of CH_4/N_2 mixtures during photochemical aerosol formation: Relevance to Titan. *Icarus* **2016**, *270*, 421−428.
(29) Sebree, J. A.; Trainer, M. G.; Loeffler, M. J.; Anderson, C. M. Titan aerosol analog absorption features produced from aromatics in the far infrared. *Icarus* **2014**, *236*, 146−152.
(30) Gautier, T.; Trainer, M. G.; Loeffler, M. J.; Sebree, J. A.; Anderson, C. M. Environmental temperature effect on the far-infrared absorption features of aromatic-based Titan's aerosol analogs. *Icarus* **2017**, *281*, 338−341.
(31) Gautier, T.; Sebree, J. A.; Li, X.; Pinnick, V. T.; Grubisic, A.; Loeffler, M. J.; Getty, S. A.; Trainer, M. G.; Brinckerhoff, W. B. Influence of trace aromatics on the chemical growth mechanisms of Titan aerosol analogues. *Planet. Space Sci.* **2017**, *140*, 27−34.
(32) Pearce, B. K. D.; Molaverdikhani, K.; Pudritz, R. E.; Henning, T.; Hébrard, E. HCN Production in Titan's Atmosphere: Coupling Quantum Chemistry and Disequilibrium Atmospheric Modeling. *Astrophys. J.* **2020**, *901*, 110.
(33) Yung, Y. L.; Allen, M.; Pinto, J. P. Photochemistry of the atmosphere of Titan - Comparison between model and observations. *Astrophys. J., Suppl. Ser.* **1984**, *55*, 465−506.
(34) Krasnopolsky, V. A. A photochemical model of Titan's atmosphere and ionosphere. *Icarus* **2009**, *201*, 226−256.
(35) Krasnopolsky, V. A. Chemical composition of Titan's atmosphere and ionosphere: Observations and the photochemical model. *Icarus* **2014**, *236*, 83−91.
(36) Vuitton, V.; Yelle, R. V.; Klippenstein, S. J.; Hörst, S. M.; Lavvas, P. Simulating the density of organic species in the atmosphere of Titan with a coupled ion-neutral photochemical model. *Icarus* **2019**, *324*, 120−197.
(37) Cottin, H.; Guan, Y. Y.; Noblet, A.; et al. The PROCESS Experiment: An Astrochemistry Laboratory for Solid and Gaseous Organic Samples in Low-Earth Orbit. *Astrobiology* **2012**, *12*, 412−425.
(38) Carrasco, N.; Cottin, H.; Cloix, M.; Jérome, M.; Bénilan, Y.; Coll, P.; Gazeau, M.-C.; Raulin, F.; Saiagh, K.; Chaput, D.; Szopa, C. The AMINO experiment: methane photolysis under Solar VUV irradiation on the EXPOSE-R facility of the International Space Station. *Int. J. Astrobiol.* **2015**, *14*, 79−87.
(39) Tran, B. N.; Joseph, J. C.; Force, M.; Briggs, R. G.; Vuitton, V.; Ferris, J. P. Photochemical processes on Titan: Irradiation of mixtures of gases that simulate Titan's atmosphere. *Icarus* **2005**, *177*, 106−115.
(40) Wilson, E. H.; Atreya, S. K. Chemical sources of haze formation in Titan's atmosphere. *Planet. Space Sci.* **2003**, *51*, 1017−1033.
(41) Lebonnois, S.; Bakes, E. L. O.; McKay, C. P. Transition from Gaseous Compounds to Aerosols in Titan's Atmosphere. *Icarus* **2002**, *159*, 505−517.
(42) Lebonnois, S. Benzene and aerosol production in Titan and Jupiter's atmospheres: a sensitivity study. *Planet. Space Sci.* **2005**, *53*, 486−497.
(43) Lavvas, P. P.; Coustenis, A.; Vardavas, I. M. Coupling photochemistry with haze formation in Titan's atmosphere, Part I: Model description. *Planet. Space Sci.* **2008**, *56*, 27−66.
(44) Lavvas, P. P.; Coustenis, A.; Vardavas, I. M. Coupling photochemistry with haze formation in Titan's atmosphere, Part II: Results and validation with Cassini/Huygens data. *Planet. Space Sci.* **2008**, *56*, 67−99.
(45) Dodonova, N. Y. Activation of nitrogen by vacuum ultraviolet radiation. *Russ. J. Phys. Chem.* **1966**, *40*, 523−524.
(46) Cable, M. L.; Hörst, S. M.; He, C.; Stockton, A. M.; Mora, M. F.; Tolbert, M. A.; Smith, M. A.; Willis, P. A. Identification of primary amines in Titan tholins using microchip nonaqueous capillary electrophoresis. *Earth Planet. Sci. Lett.* **2014**, *403*, 99−107.
(47) Yoon, Y. H.; Hörst, S.; Hicks, R.; Li, R.; de Gouw, J.; Tolbert, M. The role of benzene photolysis in Titan haze formation. *Icarus* **2014**, *233*, 233−241.
(48) Hicks, R. K.; Day, D.; Jimenez, J.; Tolbert, M. Elemental Analysis of Complex Organic Aerosol Using Isotopic Labeling and Unit-Resolution Mass Spectrometry. *Anal. Chem.* **2015**, *87*, 2741−2747.
(49) Hicks, R. K.; Day, D.; Jimenez, J.; Tolbert, M. Follow the Carbon: Isotopic Labeling Studies of Early Earth Aerosol. *Astrobiology* **2016**, *16*, 822−830.
(50) Sebree, J. A.; Roach, M. C.; Shipley, E. R.; He, C.; Hörst, S. M. Detection of Prebiotic Molecules in Plasma and Photochemical Aerosol Analogs Using GC/MS/MS Techniques. *Astrophys. J.* **2018**, *865*, 133.
(51) Hörst, S. M.; He, C.; Ugelow, M. S.; Jellinek, A. M.; Pierrehumbert, R. T.; Tolbert, M. A. Exploring the Atmosphere of Neoproterozoic Earth: The Effect of O_2 on Haze Formation and Composition. *Astrophys. J.* **2018**, *858*, 119.
(52) He, C.; Hörst, S. M.; Lewis, N. K.; Moses, J. I.; Kempton, E. M. R.; Marley, M. S.; Morley, C. V.; Valenti, J. A.; Vuitton, V. Gas Phase Chemistry of Cool Exoplanet Atmospheres: Insight from Laboratory Simulations. *ACS Earth Space Chem.* **2019**, *3*, 39−50.
(53) He, C.; Hörst, S. M.; Lewis, N. K.; Yu, X.; Moses, J. I.; McGuiggan, P.; Marley, M. S.; Kempton, E. M. R.; Morley, C. V.; Valenti, J. A.; Vuitton, V. Haze Formation in Warm H_2-rich Exoplanet Atmospheres. *Planet. Sci. J.* **2020**, *1*, 51.
(54) Ugelow, M. S.; Berry, J. L.; Browne, E. C.; Tolbert, M. A. The Impact of Molecular Oxygen on Anion Composition in a Hazy Archean Earth Atmosphere. *Astrobiology* **2020**, *20*, 658−669.
(55) Courtin, R. D.; Sim, C. K.; Kim, S. J.; Gautier, D. In *The Tropospheric Abundance of H2 on Titan from the Cassini CIRS Investigation*, AAS/Division for Planetary Sciences Meeting Abstracts #39, 2007; p 56.05.
(56) Courtin, R.; Sim, C. K.; Kim, S. J.; Gautier, D. The abundance of H_2 in Titan's troposphere from the Cassini CIRS investigation. *Planet. Space Sci.* **2012**, *69*, 89−99.
(57) Niemann, H. B.; Atreya, S. K.; Demick, J. E.; Gautier, D.; Haberman, J. A.; Harpold, D. N.; Kasprzak, W. T.; Lunine, J. I.; Owen, T. C.; Raulin, F. Composition of Titan's lower atmosphere and simple surface volatiles as measured by the Cassini-Huygens probe gas chromatograph mass spectrometer experiment. *J. Geophys. Res.: Planets* **2010**, *115*, No. E12006.
(58) Bobeldijk, M.; Kistemaker, P. G.; Boon, J. J. Testing the performance of a VUV photoionization source on a double focussing mass spectrometer using alkanes and thiophenes. *Int. J. Mass Spectrom. Ion Processes* **1991**, *110*, 179−194.
(59) Kim, Y. K.; Ali, M. A.; Rudd, M. E. Electron-Impact Total Ionization Cross Sections of CH and C_2H_2. *J. Res. Natl. Inst. Stand. Technol.* **1997**, *102*, 693−696.

https://doi.org/10.1021/acsearthspacechem.4c00102
ACS Earth Space Chem. 2024, 8, 2362−2371

(60) Tian, C.; Vidal, C. R. Electron impact dissociative ionization of ethane: Cross sections, appearance potentials, and dissociation pathways. *J. Chem. Phys.* **1998**, *109*, 1704−1712.
(61) Bettega, M. H. F.; Lima, M. A. P.; Ferreira, L. G. Scattering of low-energy electrons by isomers of C_4H_{10}. *J. Phys. B: At., Mol. Opt. Phys.* **2007**, *40*, 3015−3023.
(62) Jiao, C. Q.; DeJoseph, C. A.; Garscadden, A. Electron impact ionization and ion reactions in n-butane. *J. Phys. D: Appl. Phys.* **2007**, *40*, 409−414.
(63) Pandya, S. H.; Shelat, F. A.; Joshipura, K. N.; Vaishnav, B. G. Electron ionization of exotic molecular targets CN, C2N2, HCN, HNC and BF—Theoretical cross sections. *Int. J. Mass Spectrom.* **2012**, *323*−*324*, 28−33.
(64) Song, M.-Y.; Yoon, J.-S.; Cho, H.; Itikawa, Y.; Karwasz, G. P.; Kokoouline, V.; Nakamura, Y.; Tennyson, J. Cross Sections for Electron Collisions with Methane. *J. Phys. Chem. Ref. Data* **2015**, *44*, No. 023101.
(65) Zhou, W.; Wilkinson, L.; Lee, J. W. L.; Heathcote, D.; Vallance, C. Total electron ionization cross-sections for molecules of astrochemical interest. *Mol. Phys.* **2019**, *117*, 3066−3075.
(66) Adams, D.; Luo, Y.; Yung, Y. L. Hydrocarbon chemistry in the atmosphere of a Warmer Exo-Titan. *Front. Astron. Space Sci.* **2022**, *9*, No. 823227.
(67) Sato, K.; Misawa, K.; Kobayashi, Y.; Matsui, M.; Tsunashima, S.; Kurosaki, Y.; Takayanagi, T. Measurements of Thermal Rate Constants for the Reactions of $N(^2D,^2P)$ with C_2H_4 and C_2D_4 between 225 and 292 K. *J. Phys. Chem. A* **1999**, *103*, 8650−8656.
(68) Payne, W. A.; Monks, P. S.; Nesbitt, F. L.; Stief, L. J. The reaction between $N(^4S)$ and C_2H_3: Rate constant and primary reaction channels. *J. Chem. Phys.* **1996**, *104*, 9808−9815.
(69) Baulch, D. L.; Cobos, C. J.; Cox, R. A.; Esser, C.; Frank, P.; Just, T.; Kerr, J. A.; Pilling, M. J.; Troe, J.; Walker, R. W.; Warnatz, J. Evaluated Kinetic Data for Combustion Modelling. *J. Phys. Chem. Ref. Data* **1992**, *21*, 411−734.
(70) Knyazev, V. D.; Bencsura, À.; Stoliarov, S. I.; Slagle, I. R. Kinetics of the $C_2H_3 + H_2 \leq => H + C_2H_4$ and $CH_3 + H_2 \leq => H + CH_4$ reactions. *J. Phys. Chem. A* **1996**, *100*, 11346−11354.
(71) Lu, H.-C.; Chen, H.-K.; Cheng, B.-M. Analysis of C2H4 in C2H6 and C2H5D with VUV Absorption Spectroscopy and a Method To Remove C2H4 from C2H6 and C2H5D. *Anal. Chem.* **2004**, *76*, 5965−5967.
(72) Smith, P. L.; Yoshino, K.; Parkinson, W. H.; Ito, K.; Stark, G. High-resolution, VUV (147−201 nm) photoabsorption cross sections for C_2H_2 at 195 and 295 K. *J. Geophys. Res.* **1991**, *96*, 17529−17533.
(73) Eden, S.; Limão-Vieira, P.; Kendall, P.; Mason, N. J.; Hoffmann, S. V.; Spyrou, S. M. High resolution photo-absorption studies of acrylonitrile, C_2H_3CN, and acetonitrile, CH_3CN. *Eur. Phys. J. D* **2003**, *26*, 201−210.
(74) Lee, L. C. CN(A2πi→X2Σ+) and CN(B2Σ+→X2Σ+) yields from HCN photodissociation. *J. Chem. Phys.* **1980**, *72*, 6414−6421.
(75) Lombos, B. A.; Sauvageau, P.; Sandorfy, C. The electronic spectra of n-alkanes. *J. Mol. Spectrosc.* **1967**, *24*, 253−269.
(76) Person, J. C.; Nicole, P. P. Isotope Effects in the Photoionization Yields and the Absorption Cross Sections for Ethylene and n-Butane. *J. Chem. Phys.* **1968**, *49*, 5421−5426.
(77) Kameta, K.; Machida, S.; Kitajima, M.; Ukai, M.; Kouchi, N.; Hatano, Y.; Ito, K. Photoabsorption, photoionization, and neutral-dissociation cross sections of C2H6 and C3H8 in the extreme-uv region. *J. Electron Spectrosc. Relat. Phenom.* **1996**, *79*, 391−393.
(78) Kameta, K.; Kouchi, N.; Ukai, M.; Hatano, Y. Photoabsorption, photoionization, and neutral-dissociation cross sections of simple hydrocarbons in the vacuum ultraviolet range. *J. Electron Spectrosc. Relat. Phenom.* **2002**, *123*, 225−238.
(79) Okabe, H.; Becker, D. A. Vacuum Ultraviolet Photochemistry. VII. Photolysis of n-Butane. *J. Chem. Phys.* **1963**, *39*, 2549−2555.
(80) Chen, F. Z.; Wu, C. Y. R. Temperature-dependent photoabsorption cross sections in the VUV-UV region. l. Methane and ethane. *J. Quant. Spectrosc. Radiat. Transfer* **2004**, *85*, 195−209.
(81) Mount, G. H.; Warden, E.; Moos, H. Photoabsorption cross sections of methane from 1400 to 1850 Å. *Astrophys. J.* **1977**, *214*, L47−L49.
(82) Cheng, B.-M.; Chen, H.-F.; Lu, H.-C.; Chen, H.-K.; Alam, M. S.; Chou, S.-L.; Lin, M.-Y. Absorption Cross Section of Gaseous Acetylene at 85 K in the Wavelength Range 110−155 nm. *Astrophys. J., Suppl. Ser.* **2011**, *196*, No. 3.
(83) Gupta, S. K.; Ochiai, E.; Ponnamperuma, C. Organic synthesis in the atmosphere of Titan. *Nature* **1981**, *293*, 725−727.

https://doi.org/10.1021/acsearthspacechem.4c00102
ACS Earth Space Chem. 2024, 8, 2362−2371